Nonlinear Dynamic Modeling for a Flexible Laminated Composite Appendage Attached to a Spacecraft Body Undergoing Deployment and Locking Motions

Bin Di You[1]; Jian Min Wen[2]; Guang Yu Zhang[3]; Yang Zhao[4]

Abstract: A nonlinear dynamic modeling method is developed for a deployment and locking mechanism composed of laminated composite appendage. Unlike most formulations of linear models which ignore coupled and nonlinear terms resulting in a seriously improper response, the present model takes into account the effects of geometric nonlinearity and coupled deformations. In order to accurately obtain the dynamic response of laminated composited appendages, nonlinear strain-displacement relations for laminated plate/shell elements are presented, and the corresponding formulations are derived from the Piola–Kirchhoff stress tensor for evaluating the internal forces. Furthermore, the effect of contact and impact located at a spring hinge is investigated, which can achieve the actuating and locking functions. To study the dynamic behavior of contact-impact, the generalized contact-impact forces between the pin and locking groove are considered in the model. Meanwhile, the Jacobian matrices of geometric and momentum constraints are derived from hinge kinematics. Finally, the complete expressions including coupled deformation terms, nonlinear stiffness, additional stiffness terms, and contact-impact forces are presented, and a full analysis is achieved by using both the linear model and nonlinear model, respectively. Numerical simulation results are obtained to verify the dynamic effects of coupled deformation terms, the nonlinear stiffness and additional stiffness terms in the present model. **DOI: 10.1061/(ASCE)AS.1943-5525.0000570.**

Author keywords: Deployment and locking mechanism; Spacecraft; Laminated composite appendage; Dynamics modeling; Nonlinear properties.

Introduction

A deployment and locking mechanism is composed of flexible rotating appendages which are attached to the central rigid spacecraft body, such as a satellite antenna, space robots, solar array, and so on. For the sake of carrying capacity of space rockets, large scale, low density, low stiffness, and laminated composite materials have been widely used in the design of these appendages (Modi 1974; You et al. 2010). The appendages will experience deployment and locking motions coupled with elastic deformation, hence undesirable vibrations will take place. It can also mutually cause large attitude motions of a spacecraft body in the free-floating state (Meirovitch 1987; Meirovitch and Kwak 1989). On the other hand, the dynamics behavior of flexible appendages is coupled with large elastic deformation due to sudden contact-impact forces at the end of deployment. Therefore, the governing equations of the system are strongly nonlinear and dynamically coupled (Liu and Hong 2002, 2003, 2004). These nonlinearities present strong challenges to modeling the complete dynamic system.

Nevertheless, there are few analyses regarding the dynamic response of flexible appendages experiencing overall motions and locking motions accompanied by nonlinear elastic deformations. Thus, how to find a new efficient modeling method to accurately predict the dynamic behavior of deployment mechanism coupled with laminated composite appendages is an urgently challenging task.

In the past several decades, the previous studies in the dynamic response of flexible appendages mainly focus on analysis of linear elastic deformations of standard materials. However, the literature on precise description of flexible appendages is rather sparse, especially concerning for the laminated composite materials. Recently, most engineers and applied scientists have paid more attention to the dynamic behaviors of laminated composite appendages. Accordingly, structural vibration analyses of flexible appendages have attracted considerable interest. Harras et al. (2002) studied geometric nonlinearity of symmetrically-rectangular laminated plates for investigating the effect of nonlinear resonance frequencies (Harras et al. 2002). Messina and Soldatos presented a two-dimensional (2D) theory to account for the continuity of shear stresses in laminated plates composed of monoclinic-elastic layers (Messina and Soldatos 2002). A few investigators analyzed nonlinear-dynamic responses of internal resonance of laminated composite plate/shell structures with parametric and external excitations (Zhang 2001; Abe et al. 2000, 2007; Guo et al. 2010; Topal and Uzman 2010). The results show that the structural properties of laminated composite materials are key characteristics and they can excite undesired nonlinear oscillations. However, the previously mentioned investigators mainly studied some structure dynamics, which do not reveal the dynamic characteristics undergoing a large overall motion.

Although dynamic models for flexible multibody systems have been studied widely in the earlier stages, the dynamic analysis of

[1]Associate Professor, School of Naval Architecture and Ocean Engineering, Harbin Institute of Technology, Weihai, Shandong 264209, China.

[2]Associate Professor, School of Naval Architecture and Ocean Engineering, Harbin Institute of Technology, Weihai, Shandong 264209, China (corresponding author). E-mail: wenjm@hitwh.edu.cn

[3]Professor, School of Mechanical and Electrical Engineering, Harbin Institute of Technology, Harbin, Heilongjiang 150001, China.

[4]Professor, School of Astronautics Engineering, Harbin Institute of Technology, Harbin, Heilongjiang 150001, China.

Note. This manuscript was submitted on April 1, 2015; approved on September 1, 2015; published online on March 2, 2016. Discussion period open until August 2, 2016; separate discussions must be submitted for individual papers. This paper is part of the ***Journal of Aerospace Engineering***, © ASCE, ISSN 0893-1321.

spacecraft composed of laminated composite plates/shells has not been paid enough attention. Du et al. (1996) presented a nonlinear dynamic model for laminated beams undergoing both large overall rigid body motions and large relative elastic deflections (Du et al. 1996). Chandiramani developed a geometrically nonlinear model for a laminated, anisotropic, and composite beam (Chandiramani et al. 2002, 2003). Moreover, a few investigators studied the vibration behavior and control of deformations of laminated composite beam by using Hamilton's principle and finite element method (Baz and Ro 2001; Fung and Yau 2004; Fung et al. 2004; Lin and Chen 2003). For the same problems, extensive studies of beam-type configurations coupled with elastic deformations undergoing a large overall motion were reported. The special dynamic behaviors of laminated composite plates/shells attracted some investigators. Kremer et al. (1993a, b) discussed and analyzed the dynamic behaviors of laminated composite plates undergoing large rigid-body displacements and small elastic deformations, and presented the differences between homogeneous isotropic and laminated composite plates (Kremer et al. 1993a, b). Madenci and Barut (1996) analyzed the dynamic response of a thick laminated shell experiencing nonlinear elastic deformations coupled with a large rigid-body motion using the virtual work principle (Madenci and Barut 1996; Barut et al. 1996). Neto et al. (2004) described a multibody-based methodology for the analysis of flexible multibody systems composed of composite materials (Neto et al. 2004). Neto et al. (2006) also applied this method to analyze the deployment of synthetic aperture radar antenna (Neto et al. 2006).

However, rare studies have been reported in the literature so far about the laminated composite appendage undergoing deployment and locking motions. For most appendages of aerospace mechanism experience a locking motion at the hinges, the locking motion yields impact forces and moments between the pin and groove, and the contact-impact effects have an important influence on the attitude of the spacecraft body.

In order to precisely predict the dynamic behavior, the aim of the present investigation is to develop a dynamic model including laminated composite plates/shells undergoing deployment and locking motions. Also, the linear and angular momentum constraints and contact-impact forces acting on a hinge are obtained. Thus, the complete expressions of nonlinear terms, coupled deformation terms and contact-impact forces are developed in this study.

Rigid-Flexible Coupled Dynamic Modeling

A deployment mechanism is an assembly of spacecraft body, rigid yoke, flexible appendages, and spring hinges. The appendages employ thin and laminated composite components, and the bodies are connected by reliable spring hinges.

As the deployment angle between the yoke and appendage reaches the deployed position, the hinge is locked by a locking mechanism with a self-locking function. The configuration of the mechanism is illustrated in Fig. 1. While the flexible appendage is deployed from the stowed position, the spring hinge acts as a restoring torque for spacecraft, and the cylindrical pin slides along the locking groove. After some oscillations damped by various frictions, a static equilibrium of all the bodies and mechanisms is reached.

To obtain the dynamic models of the deployment and locking mechanism with flexible laminated composite appendages, the following assumptions were made:

1. Spacecraft body and yoke are regarded as rigid bodies except appendages which are rigidly attached to yokes by spring hinges,

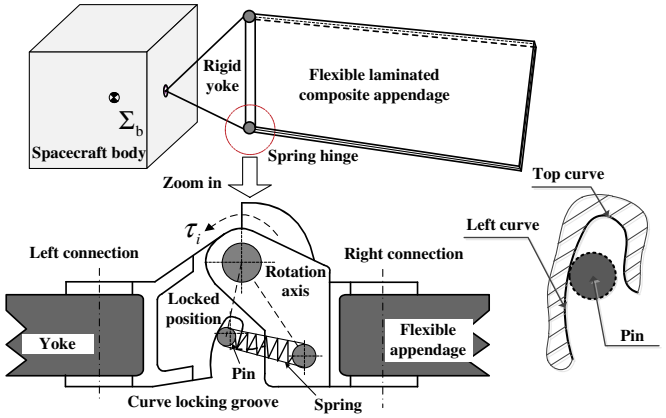

Fig. 1. Configuration of deployment and locking mechanism

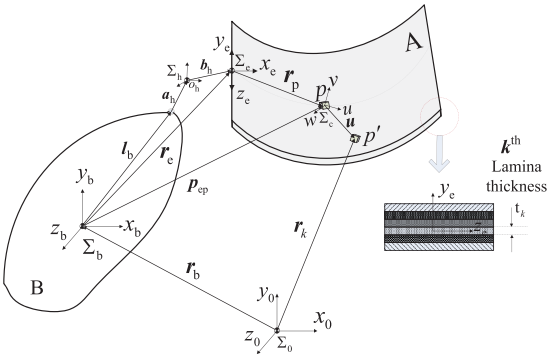

Fig. 2. Description of a deployment mechanism with flexible appendage

2. Spacecraft body is free-floating and regarded as the controllable object, and
3. Nonlinear effects of joint clearance and space microgravity are ignored.

Virtual Work by Inertial Forces

A flexible body of appendage mounted on the mechanism is considered as shown in Fig. 2. Coordinate systems are defined as follows: Inertial coordinate system is defined as Σ_0, the spacecraft body coordinate system Σ_b is attached on the base body with its origin at the centroid of the base. The hinge coordinate system is defined as Σ_h in two adjacent bodies, and the flexible appendage and its nodal coordinate system are defined as Σ_e and Σ_c, respectively. Moreover, the position vector $\boldsymbol{r}_b$ is the position of the spacecraft body in Σ_0, $\boldsymbol{r}_e$ is the displacement vector of the origin of Σ_e expressed in Σ_b, $\boldsymbol{r}_p$ is the displacement vector of point P at time t on the undeformed appendage body expressed in Σ_e, $\boldsymbol{u}$ is elastic deformation expressed in Σ_e, $\boldsymbol{l}_b$ is a vector from joint to centroid of the base, and $\boldsymbol{a}_h$ and $\boldsymbol{b}_h$ are vectors from adjacent joints to the origin of Σ_h, respectively. Referring to Fig. 2, the displacement vector $\boldsymbol{r}_e$ with respect to Σ_B can be written as $\boldsymbol{r}_e = \boldsymbol{l}_b + \boldsymbol{a}_h + \boldsymbol{b}_h$.

As shown in Fig. 2, the point P would move to point P' due to elastic deformation. The displacement vector of point P on kth layer laminated composite material appendage in Σ_0 can be written as

$$ {}^0\boldsymbol{r}_k = {}^0\boldsymbol{r}_b + {}^b\boldsymbol{r}_e + {}^e\boldsymbol{r}_p + {}^e\boldsymbol{u} \tag{1} $$

where the subscript 0, b, and e represent inertial frame, spacecraft body, and appendage, respectively. Due to the element mass dm of the undeformed appendage A is independent of time t, ${}^e\dot{\boldsymbol{r}}_p$ can be simplified into ${}^e\dot{\boldsymbol{r}}_p \equiv 0$. Differentiating Eq. (1) with respect to time and negligible time variation ${}^e\dot{\boldsymbol{r}}_p$, the velocity of point P is

$$ {}^0\dot{\boldsymbol{r}}_k = {}^0\dot{\boldsymbol{r}}_b + \boldsymbol{\omega}_b \times {}^b\boldsymbol{r}_e + \boldsymbol{\omega} \times {}^e\boldsymbol{r}_p + {}^e\dot{\boldsymbol{u}} + \boldsymbol{\omega} \times {}^e\boldsymbol{u} \tag{2} $$

where $\boldsymbol{\omega}_b$ and $\boldsymbol{\omega}$ are the angular velocity of the spacecraft body and appendage in Σ_e, respectively. And, $\boldsymbol{\omega}$ is given by

$$ \boldsymbol{\omega} = \boldsymbol{\omega}_b + \boldsymbol{\omega}_a \tag{3} $$

where $\boldsymbol{\omega}_a$ = angular velocity of the flexible appendage. By ignoring higher order term $\boldsymbol{\omega} \times {}^e\boldsymbol{u}$ according to Eq. (1), and the substitution of $\delta^0\boldsymbol{r}_b$, $\delta\boldsymbol{\Omega}_b$, $\delta\boldsymbol{\Omega}_a$, and $\delta^e\boldsymbol{u}$ for ${}^0\dot{\boldsymbol{r}}_b$, $\boldsymbol{\omega}_b$, $\boldsymbol{\omega}_a$, and ${}^e\dot{\boldsymbol{u}}$, one can get the velocity of the point P

$$ \delta^0\dot{\boldsymbol{r}}_k = \delta^0\dot{\boldsymbol{r}}_b - {}^b\boldsymbol{r}_e \times \delta\dot{\boldsymbol{\Omega}}_b - {}^e\boldsymbol{r}_p \times (\delta\dot{\boldsymbol{\Omega}}_b + \delta\dot{\boldsymbol{\Omega}}_a) + \delta^e\dot{\boldsymbol{u}} \tag{4} $$

in which ${}^e\boldsymbol{u}$ can be expressed as

$$ {}^e\boldsymbol{u} = \boldsymbol{S}_c\boldsymbol{u}'' \tag{5} $$

where $\boldsymbol{S}_c$ = interpolation matrix independent of time t; and $\boldsymbol{u}''$ is displacement vector of the elastic deformation ${}^e\boldsymbol{u}$ in Σ_c, and it is defined as $\boldsymbol{u}'' = (\,u \quad v \quad w\,)^T$.

As shown in Fig. 2, let ${}^b\boldsymbol{P}_{ep} = {}^b\boldsymbol{r}_e + {}^e\boldsymbol{r}_p$, then Eq. (4) can be expressed in terms of the matrix as

$$ \delta^0\dot{\boldsymbol{r}}_k = \delta^0\dot{\boldsymbol{r}}_b - {}^0\boldsymbol{T}_b(\boldsymbol{\Omega}){}^b\tilde{\boldsymbol{P}}_{ep}\delta\dot{\boldsymbol{\Omega}}_b - {}^0\boldsymbol{T}_e(\boldsymbol{\Omega}){}^e\tilde{\boldsymbol{r}}_p\delta\dot{\boldsymbol{\Omega}}_a + {}^0\boldsymbol{T}_e(\boldsymbol{\Omega})\boldsymbol{S}_c\delta\dot{\boldsymbol{u}}'' \tag{6} $$

where ${}^0\boldsymbol{T}_b(\boldsymbol{\Omega})$ and ${}^0\boldsymbol{T}_e(\boldsymbol{\Omega})$ are the rotation transformation matrix from Σ_b and Σ_e to Σ_0, respectively. A tilde operator denoted as subscript $\sim$ stands for a cross product such that $\tilde{\boldsymbol{r}}$is a cross product matrix of vector $\boldsymbol{r}$, i.e., $\boldsymbol{r} = [\,r_x \quad r_y \quad r_z\,]^T$ and $\tilde{\boldsymbol{r}} \overset{\text{def}}{=} \begin{bmatrix} 0 & -r_z & r_y \\ r_z & 0 & -r_x \\ -r_y & r_x & 0 \end{bmatrix}$. Thus, ${}^b\tilde{\boldsymbol{P}}_{ep}$ is the slew-symmetric matrix of ${}^b\boldsymbol{P}_{ep}$.

Differentiating Eq. (2) with respect to time, the acceleration of point P is found to be

$$ \begin{aligned} {}^0\ddot{\boldsymbol{r}}_k = {}^0\ddot{\boldsymbol{r}}_b - {}^b\boldsymbol{r}_e \times \dot{\boldsymbol{\omega}}_b - {}^e\boldsymbol{r}_p \times \dot{\boldsymbol{\omega}} + {}^e\ddot{\boldsymbol{u}} + (\boldsymbol{\omega}_b \times \boldsymbol{\omega}_b \times {}^b\boldsymbol{r}_e) + \dot{\boldsymbol{\omega}} \\ \times {}^e\boldsymbol{u} + 2\boldsymbol{\omega} \times {}^e\dot{\boldsymbol{u}} + \boldsymbol{\omega} \times \boldsymbol{\omega} \times ({}^e\boldsymbol{r}_p + {}^e\boldsymbol{u}) \end{aligned} \tag{7} $$

or, it can be rewritten in matrix form as

$$ \begin{aligned} {}^0\ddot{\boldsymbol{r}}_k = {}^0\ddot{\boldsymbol{r}}_b - {}^0\boldsymbol{T}_b{}^b\tilde{\boldsymbol{P}}_{ep}\dot{\boldsymbol{\omega}}_b - {}^0\boldsymbol{T}_e{}^e\tilde{\boldsymbol{r}}_p\boldsymbol{\Omega}_a + {}^0\boldsymbol{T}_e\boldsymbol{S}_c\ddot{\boldsymbol{u}}'' - {}^0\boldsymbol{T}_b\tilde{\boldsymbol{\omega}}_b{}^b\boldsymbol{r}_e\tilde{\boldsymbol{\omega}}_b \\ + {}^0\boldsymbol{T}_e\dot{\tilde{\boldsymbol{\omega}}}\boldsymbol{S}_c\boldsymbol{u}'' + 2{}^0\boldsymbol{T}_e\tilde{\boldsymbol{\omega}}\boldsymbol{S}_c\dot{\boldsymbol{u}}'' - {}^0\boldsymbol{T}_e\tilde{\boldsymbol{\omega}}({}^e\boldsymbol{r}_p + \boldsymbol{S}_c\boldsymbol{u}'')\tilde{\boldsymbol{\omega}} \end{aligned} \tag{8} $$

According to Eqs. (6) and (8), the virtual work δW_A can be expressed as

$$ \begin{aligned} \delta W_A = -\sum_{k=1}^{N}\int_{A_k} {}^0\ddot{\boldsymbol{r}}_k \cdot \delta^0\boldsymbol{r}_k dm = -\delta^0\boldsymbol{r}_b^T[m_A{}^0\ddot{\boldsymbol{r}}_b - {}^0\boldsymbol{T}_b\tilde{\boldsymbol{L}}_{ep}\dot{\boldsymbol{\omega}}_b \\ - {}^0\boldsymbol{T}_e\tilde{\boldsymbol{L}}_A\boldsymbol{\omega} + {}^0\boldsymbol{T}_e\boldsymbol{P}_A\boldsymbol{u}'' + {}^0\boldsymbol{T}_e(\dot{\tilde{\boldsymbol{\omega}}}\boldsymbol{P}_A\boldsymbol{u}'' + 2\tilde{\boldsymbol{\omega}}\boldsymbol{P}_A\dot{\boldsymbol{u}}'' \\ + \tilde{\boldsymbol{\omega}}\,\tilde{\boldsymbol{\omega}}\,\boldsymbol{P}_A\boldsymbol{u}'' - \tilde{\boldsymbol{\omega}}\tilde{\boldsymbol{L}}_A\boldsymbol{\omega}) + {}^0\boldsymbol{T}_b\tilde{\boldsymbol{\omega}}_b m_A{}^e\tilde{\boldsymbol{r}}_p\boldsymbol{\omega}_b] \\ - \delta\boldsymbol{\Omega}_b^T[\boldsymbol{L}_{ep}^T{}^0\boldsymbol{T}_b{}^0\ddot{\boldsymbol{r}}_b + \boldsymbol{J}_{ep}\dot{\boldsymbol{\omega}}_b + \boldsymbol{J}_{ba}\dot{\boldsymbol{\omega}}_a + \boldsymbol{J}_{bp}\boldsymbol{\omega} + \boldsymbol{H}_{ep}\ddot{\boldsymbol{u}}'' \\ + \dot{\boldsymbol{H}}_{\omega p}\boldsymbol{u}'' + 2\boldsymbol{H}_{\omega p}\dot{\boldsymbol{u}}'' + \boldsymbol{H}_{bp}\boldsymbol{u}'' + \tilde{\boldsymbol{L}}_{ep}^T\tilde{\boldsymbol{\omega}}_b{}^b\tilde{\boldsymbol{r}}_e\boldsymbol{\omega}_b] \\ - \delta\boldsymbol{\Omega}_a^T[-\boldsymbol{L}_A^T{}^0\boldsymbol{T}_e{}^0\ddot{\boldsymbol{r}}_b + \boldsymbol{J}_{ba}^T\dot{\boldsymbol{\omega}}_b + \boldsymbol{J}_A\dot{\boldsymbol{\omega}}_a + \boldsymbol{J}_{pa}\boldsymbol{\omega} + \boldsymbol{H}_A\ddot{\boldsymbol{u}}'' \\ + \dot{\boldsymbol{H}}_{\omega a}\boldsymbol{u}'' + 2\boldsymbol{H}_{\omega a}\dot{\boldsymbol{u}}'' + \boldsymbol{H}_{pa}\boldsymbol{u}'' - \boldsymbol{L}_A^{Tb}\boldsymbol{T}_e\tilde{\boldsymbol{\omega}}_b{}^b\tilde{\boldsymbol{r}}_e\boldsymbol{\omega}_b] \\ - \delta\boldsymbol{u}''^T[\boldsymbol{P}_A^{T0}\boldsymbol{T}_b{}^0\ddot{\boldsymbol{r}}_b + \boldsymbol{H}_{ep}^T\dot{\boldsymbol{\omega}}_b + \boldsymbol{H}_A^T\dot{\boldsymbol{\omega}}_a + \boldsymbol{L}_c\ddot{\boldsymbol{u}}'' + \dot{\boldsymbol{M}}_{pa}\boldsymbol{u}'' \\ + 2\boldsymbol{M}_{pa}\dot{\boldsymbol{u}}'' + \boldsymbol{M}_{ba}\boldsymbol{u}'' + \boldsymbol{H}_{ba}^T\boldsymbol{\omega} - \boldsymbol{P}_A^{Tb}\boldsymbol{T}_e\tilde{\boldsymbol{\omega}}_b{}^b\tilde{\boldsymbol{r}}_e\tilde{\boldsymbol{\omega}}_b] \end{aligned} \tag{9} $$

where m_A is the total mass of the appendage A, and $m_A = \sum_{k=1}^{N}\int_{A_k} dm$. $\tilde{\boldsymbol{L}}_{ep}$ and $\tilde{\boldsymbol{L}}_A$ are the slew-symmetric matrix of the undeformed appendage A in Σ_0 and Σ_e, respectively, $\tilde{\boldsymbol{L}}_{ep} = \sum_{k=1}^{N}\int_{A_k}{}^b\tilde{\boldsymbol{P}}_{ep}dm$ and $\tilde{\boldsymbol{L}}_A = \sum_{k=1}^{N}\int_{A_k}{}^e\tilde{\boldsymbol{r}}_p dm$. $\boldsymbol{P}_A$ is the matrix of momentum coefficient for appendage A, $\boldsymbol{P}_A = \sum_{k=1}^{N}\int_{A_k}\boldsymbol{S}_c dm$. $\boldsymbol{J}_{ep}$ and $\boldsymbol{J}_A$ are the inertia matrix of the undeformed appendage A in Σ_b and Σ_e respectively, $\boldsymbol{J}_{ep} = \sum_{k=1}^{N}\int_{A_k}{}^b\tilde{\boldsymbol{P}}_{ep}^T{}^b\tilde{\boldsymbol{P}}_{ep}dm$ and $\boldsymbol{J}_A = \sum_{k=1}^{N}\int_{A_k}{}^e\tilde{\boldsymbol{r}}_p^T{}^e\tilde{\boldsymbol{r}}_p dm$. $\boldsymbol{J}_{ba}$ is the coupled inertia matrix, $\boldsymbol{J}_{ba} = {}^b\boldsymbol{r}_e^{Tb}\boldsymbol{T}_e\tilde{\boldsymbol{L}}_A + {}^b\boldsymbol{T}_e\boldsymbol{J}_A$. And the remaining sub-matrix of the block matrix can be obtained from the following equations: $\boldsymbol{J}_{bp} = \sum_{k=1}^{N}\int_{A_k}\tilde{\boldsymbol{L}}_{ep}{}^b\boldsymbol{T}_e\tilde{\boldsymbol{\omega}}{}^e\tilde{\boldsymbol{r}}_p dm$; $\boldsymbol{H}_{ep} = \sum_{k=1}^{N}\int_{A_k}\tilde{\boldsymbol{L}}_{ep}{}^b\boldsymbol{T}_e\boldsymbol{S}_c dm$; $\boldsymbol{H}_{\omega p} = \sum_{k=1}^{N}\int_{A_k}\tilde{\boldsymbol{L}}_{ep}{}^b\boldsymbol{T}_e\tilde{\boldsymbol{\omega}}\boldsymbol{S}_c dm$; $\boldsymbol{H}_{bp} = \sum_{k=1}^{N}\int_{A_k}\tilde{\boldsymbol{L}}_{ep}{}^b\boldsymbol{T}_e\tilde{\boldsymbol{\omega}}\,\tilde{\boldsymbol{\omega}}\,\boldsymbol{S}_c dm$; $\boldsymbol{J}_{pa} = \sum_{k=1}^{N}\int_{A_k}\tilde{\boldsymbol{L}}_{ep}\tilde{\boldsymbol{\omega}}\tilde{\boldsymbol{L}}_{ep}dm$; $\boldsymbol{H}_A = \sum_{k=1}^{N}\int_{A_k}{}^e\tilde{\boldsymbol{r}}_p^T\boldsymbol{S}_c dm$; $\boldsymbol{H}_{\omega a} = \sum_{k=1}^{N}\int_{A_k}\tilde{\boldsymbol{L}}_{ep}\tilde{\boldsymbol{\omega}}\boldsymbol{S}_c dm$; $\boldsymbol{H}_{pa} = \sum_{k=1}^{N}\int_{A_k}\tilde{\boldsymbol{L}}_{ep}\tilde{\boldsymbol{\omega}}\,\tilde{\boldsymbol{\omega}}\,\boldsymbol{S}_c dm$; $\boldsymbol{L}_c = \sum_{k=1}^{N}\int_{A_k}\boldsymbol{S}_c^T\boldsymbol{S}_c dm$; $\boldsymbol{M}_{pa} = \sum_{k=1}^{N}\int_{A_k}\boldsymbol{S}_c^T\tilde{\boldsymbol{\omega}}\boldsymbol{S}_c dm$; $\boldsymbol{M}_{ba} = \sum_{k=1}^{N}\int_{A_k}\boldsymbol{S}_c^T\tilde{\boldsymbol{\omega}}\,\tilde{\boldsymbol{\omega}}\,\boldsymbol{S}_c dm$; and $\boldsymbol{H}_{ba} = \sum_{k=1}^{N}\int_{A_k}{}^e\tilde{\boldsymbol{r}}_p^T\tilde{\boldsymbol{\omega}}\boldsymbol{S}_c dm$.

On the other hand, the virtual work δW_B by inertial forces of the spacecraft body can be expressed as

$$ \delta W_B = -\delta^0\boldsymbol{r}_b^T m_B{}^0\ddot{\boldsymbol{r}}_b - \delta\boldsymbol{\Omega}_b^T\boldsymbol{J}_b\delta\ddot{\boldsymbol{\Omega}}_b \tag{10} $$

where m_B and $\boldsymbol{J}_b$ are the mass and rotational inertia of rigid body spacecraft, respectively.

Combining Eqs. (9) and (10) leads to virtual work δW_I for the system by inertia forces as following equation:

$$ \delta W_I = \delta W_A + \delta W_B \tag{11} $$

Virtual work by internal forces of laminated composite appendage.

As shown in Fig. 3, the internal virtual work δW_U for the appendage can be expressed as

$$ \delta W_U = \sum_{k=1}^{N}\int_{V_k} \delta_t\boldsymbol{\varepsilon}_k^T{}_t\boldsymbol{\sigma}_k dV_k \tag{12} $$

where ${}_t\boldsymbol{\varepsilon}_k$ and ${}_t\boldsymbol{\sigma}_k$ are strain and stress tensor for the kth layer laminated structure at time t, respectively. In addition, the Green's strain components ${}_t\boldsymbol{\varepsilon}_k$ can be represented in terms of the linear and nonlinear parts of the strain tensor as

$$ {}_t\boldsymbol{\varepsilon}_k = {}_t\boldsymbol{\varepsilon}_k^L + {}_t\boldsymbol{\varepsilon}_k^{NL} \tag{13} $$

in which ${}_t\boldsymbol{\varepsilon}_k^L$ and ${}_t\boldsymbol{\varepsilon}_k^{NL}$ are the linear and nonlinear strain tensor. Accordingly

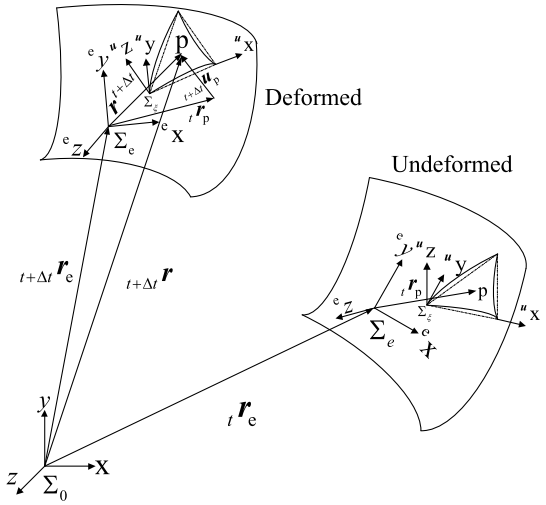

Fig. 3. Description of an arbitrary point on plate/shell structures

$$
{}_t\boldsymbol{\varepsilon}_k^L = \begin{pmatrix} \dfrac{\partial u}{\partial x} \\ \dfrac{\partial v}{\partial y} \\ \dfrac{\partial u}{\partial y} + \dfrac{\partial v}{\partial x} \end{pmatrix} + \begin{pmatrix} \dfrac{\partial \varphi_x}{\partial x} \\ \dfrac{\partial \varphi_y}{\partial y} \\ \dfrac{\partial \varphi_x}{\partial y} + \dfrac{\partial \varphi_y}{\partial x} \end{pmatrix};
$$

$$
{}_t\boldsymbol{\varepsilon}_k^{NL} = \frac{1}{2}\begin{Bmatrix} \left(\dfrac{\partial u}{\partial x}\right)^2 + \left(\dfrac{\partial v}{\partial x}\right)^2 + \left(\dfrac{\partial w}{\partial x}\right)^2 \\ \left(\dfrac{\partial u}{\partial y}\right)^2 + \left(\dfrac{\partial v}{\partial y}\right)^2 + \left(\dfrac{\partial w}{\partial y}\right)^2 \\ 2\left(\dfrac{\partial u}{\partial x}\dfrac{\partial u}{\partial y} + \dfrac{\partial v}{\partial x}\dfrac{\partial v}{\partial y} + \dfrac{\partial w}{\partial x}\dfrac{\partial w}{\partial y}\right) \end{Bmatrix} \tag{14}
$$

For solving nonlinear equations, the Piola–Kirchhoff stress components ${}_t\boldsymbol{\sigma}_k$ can be decomposed as

$$
{}_t\boldsymbol{\sigma}_k = {}_t\boldsymbol{s}_k + {}_t\Delta\boldsymbol{s}_k \tag{15}
$$

where ${}_t\boldsymbol{s}_k$ = Cauchy stress components evaluated at time t; and ${}_t\Delta\boldsymbol{s}_k$ = incremental Piola-Kirchhoff stress vector for the kth layer laminated structure between t and $t + \Delta t$.

In order to solve the nonlinear equations, the unknown incremental high-order terms are neglected for linear analysis. Namely, the linear stress-strain relations as given by

$$
\delta_t\boldsymbol{\varepsilon}_k^T{}_t\Delta\boldsymbol{s}_k \cong \delta({}_t\boldsymbol{\varepsilon}_k^L)^T{}_t\Delta\boldsymbol{s}; \qquad {}_t\Delta\boldsymbol{s}_k = \boldsymbol{Q}_k{}_t\boldsymbol{\varepsilon}_k \cong \boldsymbol{Q}_k{}_t\boldsymbol{\varepsilon}_k^L \tag{16}
$$

where $\boldsymbol{Q}_k$ represents the constitutive matrix.

By substituting Eqs. (13)–(16) into Eq. (12), the virtual work δW_U results in

$$
\delta W_U = \sum_{k=1}^{N}\int_{V_k}\delta({}_t\boldsymbol{\varepsilon}_k^L)^T\boldsymbol{Q}_k{}_t\boldsymbol{\varepsilon}_k^L dV_k + \sum_{k=1}^{N}\int_{V_k}\delta({}_t\boldsymbol{\varepsilon}_k^{\mathrm{NL}})^T{}_t\boldsymbol{s}_k dV_k + \sum_{k=1}^{N}\int_{V_k}\delta({}_t\boldsymbol{\varepsilon}_k^L)^T{}_t\boldsymbol{s}_k dV_k \tag{17}
$$

The stress-strain relation given by Eq. (5) and Eq. (14) can be obtained from

$$
{}_t\boldsymbol{\varepsilon}_k^L = \mathbb{B}\boldsymbol{u}'' \tag{18}
$$

where $\mathbb{B}$ is the strain-displacement transformation matrix. Then, the first integral in Eq. (17) can be written in terms of the total nodal vector as

$$
\sum_{k=1}^{N}\int_{V_k}\delta({}_t\boldsymbol{\varepsilon}_k^L)^T\boldsymbol{Q}_k{}_t\boldsymbol{\varepsilon}_k^L dV_k = \delta\boldsymbol{u}''^T\boldsymbol{K}_L\boldsymbol{u}'' \tag{19}
$$

in which $\boldsymbol{K}_L = \sum_{k=1}^{N}\int_{V_k}\mathbb{B}^T\boldsymbol{Q}_k\mathbb{B}dV_k$.

In addition, the nonlinear strain tensor ${}_t\boldsymbol{\varepsilon}_k^{NL}$ can be expressed as

$$
\{\,({}_t\boldsymbol{\varepsilon}_k^{NL})^T \quad \boldsymbol{0}^T\,\} = \frac{1}{2}\boldsymbol{T}_{NL}\boldsymbol{\Psi}_{NL} \tag{20}
$$

in which $\boldsymbol{\Psi}_{NL}^T = \{\frac{\partial u}{\partial x} \;\; \frac{\partial v}{\partial x} \;\; \frac{\partial w}{\partial x} \;\; \frac{\partial u}{\partial y} \;\; \frac{\partial v}{\partial y} \;\; \frac{\partial w}{\partial y}\} = \mathbb{D}\boldsymbol{u}''$; and $\mathbb{D}$ is a matrix differential operator. Furthermore, $\mathbb{D}$ and $\boldsymbol{T}_{NL}$ are defined respectively as $\mathbb{D}^T = \begin{pmatrix} \frac{\partial}{\partial x} & 0 & 0 & \frac{\partial}{\partial y} & 0 & 0 \\ 0 & \frac{\partial}{\partial x} & 0 & 0 & \frac{\partial}{\partial y} & 0 \\ 0 & 0 & \frac{\partial}{\partial x} & 0 & 0 & \frac{\partial}{\partial y} \end{pmatrix}$; and $\boldsymbol{T}_{NL} = \begin{bmatrix} \frac{\partial u}{\partial x} & \frac{\partial v}{\partial x} & \frac{\partial w}{\partial x} & 0 & 0 & 0 \\ 0 & 0 & 0 & \frac{\partial u}{\partial y} & \frac{\partial v}{\partial y} & \frac{\partial w}{\partial y} \\ \frac{\partial u}{\partial y} & \frac{\partial v}{\partial y} & \frac{\partial w}{\partial y} & \frac{\partial u}{\partial x} & \frac{\partial v}{\partial x} & \frac{\partial w}{\partial x} \\ 0 & 0 & 0 & 0 & 0 & 0 \\ 0 & 0 & 0 & 0 & 0 & 0 \\ 0 & 0 & 0 & 0 & 0 & 0 \end{bmatrix}$. According to the irrespective of the type of element, the following properties are observed based on certain algebraic manipulations

$$
\delta\boldsymbol{T}_{NL}\boldsymbol{\Psi}_{NL} = \boldsymbol{T}_{NL}\delta\boldsymbol{\Psi}_{NL}; \qquad \boldsymbol{T}_{NL}^T{}_t\boldsymbol{s}_k = \boldsymbol{N}_s\boldsymbol{\Psi}_{NL} = \boldsymbol{N}_s\mathbb{D}\boldsymbol{u}'' \tag{21}
$$

where the matrix $\boldsymbol{N}_s$ is consist of components of either stress or their resultants.

Substituting Eq. (20) into the second integral in Eq. (17), and combining with properties in Eq. (21) will result in

$$
\sum_{k=1}^{N}\int_{V_k}\delta({}_t\boldsymbol{\varepsilon}_k^{NL})^T{}_t\boldsymbol{s}_k dV_k = \delta\boldsymbol{u}''^T\boldsymbol{K}_s\boldsymbol{u}'' \tag{22}
$$

where $\boldsymbol{K}_s$ is the geometric nonlinear stiffness matrix $\boldsymbol{K}_s = \sum_{k=1}^{N}\int_{V_k}\mathbb{D}^T\boldsymbol{N}_s\mathbb{D}dV_k$; and it takes into account the effect of stress stiffening.

Similarly, the third integral in Eq. (17) can be expressed as

$$
\sum_{k=1}^{N}\int_{V_k}\delta({}_t\boldsymbol{\varepsilon}_k^L)^T{}_t\boldsymbol{s}_k dV_k = \delta\boldsymbol{u}''^T\boldsymbol{K}_L^*\boldsymbol{u}''^* \tag{23}
$$

where $\boldsymbol{K}_L^* = \boldsymbol{K}_L$; and $\boldsymbol{u}''^*$ = vector of nodal displacement with respect to local deformations between the initial and the deformed configurations of the shell elements. It is determined by subtracting the rigid-body motion from the total displacement.

Combining Eqs. (19), (22), and (23), and let $\boldsymbol{q} = [{}^0\boldsymbol{r}_b \quad \boldsymbol{\Omega}_b \quad \boldsymbol{\Omega}_a \quad \boldsymbol{u}'']^T$ as generalized coordinates for the deployment mechanism, the virtue work by internal forces in the kth element of laminated composite appendage can be expressed in matrix form as

$$
\delta W_U = \delta\boldsymbol{q}^T\boldsymbol{f}_\sigma \tag{24}
$$

where $\boldsymbol{f}_\sigma$ is the internal force vector on the flexible appendage, and $\boldsymbol{f}_\sigma = \begin{bmatrix} \mathbf{0} & \mathbf{0} & \mathbf{0} & \mathbf{0} \\ \mathbf{0} & \mathbf{0} & \mathbf{0} & \mathbf{0} \\ \mathbf{0} & \mathbf{0} & \mathbf{0} & \mathbf{0} \\ \mathbf{0} & \mathbf{0} & \mathbf{0} & \boldsymbol{K}_L + \boldsymbol{K}_s \end{bmatrix} \boldsymbol{q} + \begin{Bmatrix} \mathbf{0} \\ \mathbf{0} \\ \mathbf{0} \\ \boldsymbol{K}_L^* \boldsymbol{u}'^{/*} \end{Bmatrix}$.

Virtual Work by External Forces

The virtual work δW_E by external forces and moments is expressed as

$$\delta W_E = \delta \boldsymbol{q}^T \boldsymbol{Q} \tag{25}$$

where $\boldsymbol{Q}$ is the vector of generalized external forces, which is defined as $\boldsymbol{Q} = [\boldsymbol{Q}_0 \quad \boldsymbol{Q}_b \quad \boldsymbol{Q}_a \quad \boldsymbol{Q}_u]^T$; and $\boldsymbol{Q}_0$, $\boldsymbol{Q}_b$, $\boldsymbol{Q}_a$ and $\boldsymbol{Q}_u$ are sub-vectors of the external load block vectors acting on the dependent coordinates of the deployment mechanism.

Equations of Coupled Nonlinear Dynamics

By using the principle of virtual work

$$\delta W_I + \delta W_U + \delta W_E = 0 \tag{26}$$

and substituting Eqs. (11), (24), and (25) into Eq. (26), the dynamic model of the deployment mechanism with laminated composite appendages is given by

$$\boldsymbol{M}\ddot{\boldsymbol{q}} + \boldsymbol{K}\boldsymbol{q} = \boldsymbol{Q} - \boldsymbol{Q}_N \tag{27}$$

where $\boldsymbol{M}$ is generalized mass matrix; $\boldsymbol{K}$ is generalized stiffness matrix; and $\boldsymbol{Q}_N$ is the nonlinear term of external force and moment vectors. And,

$$\boldsymbol{M} = \begin{bmatrix} m\mathbf{E}^{3\times3} & -{}^0\boldsymbol{T}_b\tilde{\boldsymbol{L}}_{ep} & {}^0\boldsymbol{T}_e\tilde{\boldsymbol{L}}_A & {}^0\boldsymbol{T}_e\boldsymbol{P}_A \\ \boldsymbol{L}_{ep}^T{}^0\boldsymbol{T}_b & \boldsymbol{J}_{ep} + \boldsymbol{J}_b & \boldsymbol{J}_{ba} & \boldsymbol{H}_{ep} \\ -\boldsymbol{L}_A^{T0}\boldsymbol{T}_e & \boldsymbol{J}_{ba}^T & \boldsymbol{J}_A & \boldsymbol{H}_A \\ \boldsymbol{P}_A^{T0}\boldsymbol{T}_b & \boldsymbol{H}_{ep}^T & \boldsymbol{H}_A^T & \boldsymbol{L}_c \end{bmatrix} \tag{28}$$

in which the generalized mass matrix $\boldsymbol{M}$ in Eq. (28) is a symmetric matrix, that is

$$\boldsymbol{M} = \boldsymbol{M}^T \tag{29}$$

and

$$\boldsymbol{K} = \mathrm{diag}\{\, \mathbf{0} \quad \mathbf{0} \quad \mathbf{0} \quad \boldsymbol{K}_L + \boldsymbol{K}_s \,\} \tag{30}$$

$$\boldsymbol{Q}_N = \begin{Bmatrix} \boldsymbol{Q}_{Nr} \\ \boldsymbol{Q}_{Nb} \\ \boldsymbol{Q}_{Na} \\ \boldsymbol{Q}_{Nu} \end{Bmatrix} = \begin{Bmatrix} {}^0\boldsymbol{T}_e(\dot{\tilde{\boldsymbol{\omega}}}\boldsymbol{P}_A\boldsymbol{u}'' + 2\tilde{\boldsymbol{\omega}}\boldsymbol{P}_A\dot{\boldsymbol{u}}'' + \tilde{\boldsymbol{\omega}}\,\tilde{\boldsymbol{\omega}}\,\boldsymbol{P}_A\boldsymbol{u}'' - \tilde{\boldsymbol{\omega}}\tilde{\boldsymbol{L}}_A\boldsymbol{\omega}) + {}^0\boldsymbol{T}_b\tilde{\boldsymbol{\omega}}_b m_A{}^e\tilde{\boldsymbol{r}}_p\boldsymbol{\omega}_b \\ \boldsymbol{J}_{bp}\boldsymbol{\omega} + \dot{\boldsymbol{H}}_{\omega p}\boldsymbol{u}'' + 2\boldsymbol{H}_{\omega p}\dot{\boldsymbol{u}}'' + \boldsymbol{H}_{bp}\boldsymbol{u}'' + \tilde{\boldsymbol{L}}_{ep}^T\tilde{\boldsymbol{\omega}}_b{}^b\tilde{\boldsymbol{r}}_e\boldsymbol{\omega}_b \\ \boldsymbol{J}_{pa}\boldsymbol{\omega} + \boldsymbol{H}_A\boldsymbol{u}'' + \dot{\boldsymbol{H}}_{\omega a}\boldsymbol{u}'' + 2\boldsymbol{H}_{\omega a}\dot{\boldsymbol{u}}'' + \boldsymbol{H}_{pa}\boldsymbol{u}'' - \boldsymbol{L}_A^{Tb}\boldsymbol{T}_a\tilde{\boldsymbol{\omega}}_b{}^b\tilde{\boldsymbol{r}}_e\boldsymbol{\omega}_b \\ \dot{\boldsymbol{M}}_{pa}\boldsymbol{u}'' + 2\boldsymbol{M}_{pa}\dot{\boldsymbol{u}}'' + \boldsymbol{M}_{ba}\boldsymbol{u}'' + \boldsymbol{H}_{ba}^T\boldsymbol{\omega} - \boldsymbol{P}_A^{Tb}\boldsymbol{T}_a\tilde{\boldsymbol{\omega}}_b{}^b\tilde{\boldsymbol{r}}_e\tilde{\boldsymbol{\omega}}_b \end{Bmatrix} + \begin{Bmatrix} \mathbf{0} \\ \mathbf{0} \\ \mathbf{0} \\ \boldsymbol{K}_L^*\boldsymbol{u}'^{/*} \end{Bmatrix} \tag{31}$$

where m = total mass of the system; and $\mathbf{E}^{3\times3}$ = 3×3 identity matrix.

Effect of Contact-Impact in the Locking Hinge

As shown in Fig. 1, the torsional spring located at the hinge represents the appendage flexibility connecting to yoke. When the flexible appendages are deployed from the stowed position, the spring hinges act as a restoring torque for the flexible appendages. And, the torsional spring torque is defined as $\tau = \tau_0 - k\theta$, where τ_0 is a preload torque, k is a spring coefficient, and θ is a deployment angle. The effect of contact and impact is activated as deployed condition achieved, and the contact-impact force model is established as illustrated in Fig. 4, in which K_c and D_c are equivalent contact stiffness and damping, respectively.

As shown in Fig. 1, assuming the contact-impact takes place between the pin and curve locking groove when the motion of appendage approaches to the deployed position, the constraint forces will act on both bodies. It is assumed that the pin moves on the surface of the locking groove and the pin and the groove will contact with each other, and the profile of this surface is known and defined as

$$\boldsymbol{\varphi} = f(\boldsymbol{q}) \tag{32}$$

Then, the motion of appendage is subjected to the following kinematic constraints as

$$\boldsymbol{\Phi}_1(\boldsymbol{\varphi}) = \mathbf{0} \tag{33}$$

where $\boldsymbol{\Phi}_1(\boldsymbol{\varphi})$ is assumed to be twice differentiable. Now differentiating Eqs. (32) and (33) with respect to time and applying the chain rule yields

$$\left[\frac{\partial \boldsymbol{\Phi}_1(\boldsymbol{\varphi})}{\partial \boldsymbol{\varphi}} \frac{\partial f(\boldsymbol{q})}{\partial \boldsymbol{q}}\right]\dot{\boldsymbol{q}} = \boldsymbol{S}_q(\boldsymbol{q})\dot{\boldsymbol{q}} = \mathbf{0} \tag{34}$$

where the matrix $\boldsymbol{S}_q(\boldsymbol{q}) = [\partial \boldsymbol{\Phi}_1(\varphi)/\partial\varphi]\,[\partial f(\boldsymbol{q})/\partial \boldsymbol{q}]$ is the Jacobian matrix.

Combining Eqs. (2) and (3), one can obtain the linear velocity $\dot{\boldsymbol{r}}_i$ and angular velocity $\boldsymbol{\omega}_i$ of arbitrary point in matrix form as

$$\begin{pmatrix} \dot{\boldsymbol{r}}_i \\ \boldsymbol{\omega}_i \end{pmatrix} = \begin{pmatrix} \mathbf{E}^{3\times3} & -{}^0\boldsymbol{T}_b{}^b\tilde{\boldsymbol{P}}_{ep} \\ \mathbf{0} & \mathbf{E}^{3\times3} \end{pmatrix} \begin{pmatrix} {}^0\dot{\boldsymbol{r}}_b \\ \dot{\boldsymbol{\Omega}}_b \end{pmatrix} + \begin{pmatrix} -{}^0\boldsymbol{T}_e{}^e\tilde{\boldsymbol{r}}_p & {}^0\boldsymbol{T}_e\boldsymbol{S}_c \\ \mathbf{E}^{3\times3} & \mathbf{0} \end{pmatrix} \begin{pmatrix} \dot{\boldsymbol{\Omega}}_a \\ \dot{\boldsymbol{u}}'' \end{pmatrix} \tag{35}$$

Note that the linear and angular momentum be assumed as zero in initial conditions ($\boldsymbol{P} = \mathbf{0}$, $\boldsymbol{H} = \mathbf{0}$) and no external forces and torques are exerted on the whole system. The linear and angular momentums are conserved. Thus, the linear momentum $\boldsymbol{P}$ and angular momentum $\boldsymbol{H}$ are given by

$$\boldsymbol{P} = m_b\dot{\boldsymbol{r}}_b + \sum_{k=1}^{N}\int_{A_k}\dot{\boldsymbol{r}}_i dm = \mathbf{0} \tag{36}$$

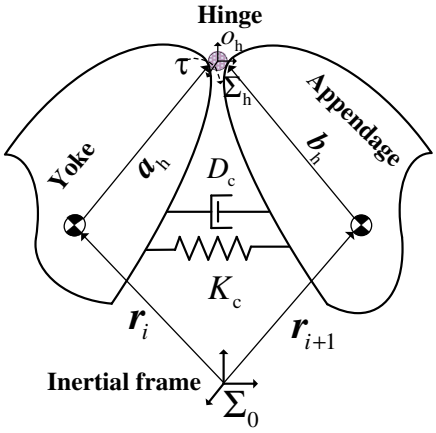

Fig. 4. Equivalent model of contact-impact force

$$\boldsymbol{H} = \boldsymbol{J}_b\boldsymbol{\omega}_b + \boldsymbol{J}_A\boldsymbol{\omega} + \sum_{k=1}^{N}\int_{A_k} \boldsymbol{r}_i \times \dot{\boldsymbol{r}}_i dm = \boldsymbol{0} \tag{37}$$

Substituting Eq. (35) into Eqs. (36) and (37), respectively, the linear momentum $\boldsymbol{P}$ angular momentum $\boldsymbol{H}$ can be represented as

$$\begin{aligned}\boldsymbol{P} &= m_b{}^0\dot{\boldsymbol{r}}_b + \sum_{k=1}^{N}\int_{A_k}({}^0\dot{\boldsymbol{r}}_b - {}^0\boldsymbol{T}_b{}^b\tilde{\boldsymbol{P}}_{ep}\dot{\boldsymbol{\Omega}}_b - {}^0\boldsymbol{T}_e{}^e\tilde{\boldsymbol{r}}_p\dot{\boldsymbol{\Omega}}_a \\ &\quad + {}^0\boldsymbol{T}_e\boldsymbol{S}_c\dot{\boldsymbol{u}}'')dm = m{}^0\dot{\boldsymbol{r}}_b + \sum_{k=1}^{N}\int_{A_k}(-{}^0\boldsymbol{T}_b{}^b\tilde{\boldsymbol{P}}_{ep}\dot{\boldsymbol{\Omega}}_b - {}^0\boldsymbol{T}_e{}^e\tilde{\boldsymbol{r}}_p\dot{\boldsymbol{\Omega}}_a \\ &\quad + {}^0\boldsymbol{T}_e\boldsymbol{S}_c\dot{\boldsymbol{u}}'')dm = \boldsymbol{0}\end{aligned} \tag{38}$$

$$\begin{aligned}\boldsymbol{H} &= \boldsymbol{J}_b\boldsymbol{\omega}_b + \boldsymbol{J}_A\boldsymbol{\omega} + \sum_{k=1}^{N}\int_{A_k}\boldsymbol{r}_i \times \left[\begin{pmatrix}\mathbf{E}^{3\times3} & -{}^0\boldsymbol{T}_b{}^b\tilde{\boldsymbol{P}}_{ep}\end{pmatrix}\begin{pmatrix}{}^0\dot{\boldsymbol{r}}_b\\ \dot{\boldsymbol{\Omega}}_b\end{pmatrix}\right. \\ &\quad \left. + \begin{pmatrix}-{}^0\boldsymbol{T}_e{}^e\tilde{\boldsymbol{r}}_p & {}^0\boldsymbol{T}_e\boldsymbol{S}_c\end{pmatrix}\begin{pmatrix}\dot{\boldsymbol{\Omega}}_a\\ \dot{\boldsymbol{u}}''\end{pmatrix}\right]dm = \boldsymbol{J}_b\boldsymbol{\omega}_b + \boldsymbol{J}_A\boldsymbol{\omega} \\ &\quad + \sum_{k=1}^{N}\int_{A_k}(\boldsymbol{r}_i - \boldsymbol{r}_b)\times\left[\begin{pmatrix}\mathbf{E}^{3\times3} & -{}^0\boldsymbol{T}_b{}^b\tilde{\boldsymbol{P}}_{ep}\end{pmatrix}\begin{pmatrix}{}^0\dot{\boldsymbol{r}}_b\\ \dot{\boldsymbol{\Omega}}_b\end{pmatrix}\right. \\ &\quad \left. + \begin{pmatrix}-{}^0\boldsymbol{T}_e{}^e\tilde{\boldsymbol{r}}_p & {}^0\boldsymbol{T}_e\boldsymbol{S}_c\end{pmatrix}\begin{pmatrix}\dot{\boldsymbol{\Omega}}_a\\ \dot{\boldsymbol{u}}''\end{pmatrix}\right]dm + \sum_{k=1}^{N}\int_{A_k}\boldsymbol{r}_b \\ &\quad \times\left[\begin{pmatrix}\mathbf{E}^{3\times3} & -{}^0\boldsymbol{T}_b{}^b\tilde{\boldsymbol{P}}_{ep}\end{pmatrix}\begin{pmatrix}{}^0\dot{\boldsymbol{r}}_b\\ \dot{\boldsymbol{\Omega}}_b\end{pmatrix}\right. \\ &\quad \left. + \begin{pmatrix}-{}^0\boldsymbol{T}_e{}^e\tilde{\boldsymbol{r}}_p & {}^0\boldsymbol{T}_e\boldsymbol{S}_c\end{pmatrix}\begin{pmatrix}\dot{\boldsymbol{\Omega}}_a\\ \dot{\boldsymbol{u}}''\end{pmatrix}\right]dm = \boldsymbol{0}\end{aligned} \tag{39}$$

According to Eq. (35) and initial conditions $\boldsymbol{P} = \boldsymbol{0}$, one can rewrite the Eq. (38) as

$$\begin{aligned}&\sum_{k=1}^{N}\int_{A_k}\boldsymbol{r}_b\times\left[\begin{pmatrix}\mathbf{E}^{3\times3} & -{}^0\boldsymbol{T}_b{}^b\tilde{\boldsymbol{P}}_{ep}\end{pmatrix}\begin{pmatrix}{}^0\dot{\boldsymbol{r}}_b\\ \dot{\boldsymbol{\Omega}}_b\end{pmatrix}\right. \\ &\quad \left. + \begin{pmatrix}-{}^0\boldsymbol{T}_e{}^e\tilde{\boldsymbol{r}}_p & {}^0\boldsymbol{T}_e\boldsymbol{S}_c\end{pmatrix}\begin{pmatrix}\dot{\boldsymbol{\Omega}}_a\\ \dot{\boldsymbol{u}}''\end{pmatrix}\right]dm + \boldsymbol{r}_b\times m_b{}^0\dot{\boldsymbol{r}}_b - \boldsymbol{r}_b \\ &\quad \times m_b{}^0\dot{\boldsymbol{r}}_b = \boldsymbol{r}_b\times\boldsymbol{P} - \boldsymbol{r}_b\times m_b{}^0\dot{\boldsymbol{r}}_b = -\tilde{\boldsymbol{r}}_b m_b{}^0\dot{\boldsymbol{r}}_b\end{aligned} \tag{40}$$

And Eq. (39) can be simplified to

$$\begin{aligned}\boldsymbol{H} &= \boldsymbol{J}_b\boldsymbol{\omega}_b + \boldsymbol{J}_A\boldsymbol{\omega} + \sum_{k=1}^{N}\int_{A_k}\boldsymbol{r}_{ib}\times\left[\begin{pmatrix}\mathbf{E}^{3\times3} & -{}^0\boldsymbol{T}_b{}^b\tilde{\boldsymbol{P}}_{ep}\end{pmatrix}\begin{pmatrix}{}^0\dot{\boldsymbol{r}}_b\\ \dot{\boldsymbol{\Omega}}_b\end{pmatrix}\right. \\ &\quad \left. + \begin{pmatrix}-{}^0\boldsymbol{T}_e{}^e\tilde{\boldsymbol{r}}_p & {}^0\boldsymbol{T}_e\boldsymbol{S}_c\end{pmatrix}\begin{pmatrix}\dot{\boldsymbol{\Omega}}_a\\ \dot{\boldsymbol{u}}''\end{pmatrix}\right]dm - \tilde{\boldsymbol{r}}_b m_b{}^0\dot{\boldsymbol{r}}_b = \boldsymbol{0}\end{aligned} \tag{41}$$

in which $\boldsymbol{r}_{ib} = \boldsymbol{r}_i - \boldsymbol{r}_b$. Then, Eqs. (38) and (41) can be rewritten in matrix form as

$$\begin{aligned}\begin{pmatrix}\boldsymbol{0}\\ \boldsymbol{0}\end{pmatrix} = \begin{pmatrix}\boldsymbol{P}\\ \boldsymbol{H}\end{pmatrix} &= \begin{pmatrix}m\mathbf{E}_3 & -\boldsymbol{H}_{Tb}\\ -\tilde{\boldsymbol{r}}_b m_b + \boldsymbol{J}_{Tb} & \boldsymbol{J}_b + \boldsymbol{J}_A - \boldsymbol{J}_{\Omega b}\end{pmatrix}\begin{pmatrix}{}^0\dot{\boldsymbol{r}}_b\\ \dot{\boldsymbol{\Omega}}_b\end{pmatrix} \\ &\quad + \begin{pmatrix}-\boldsymbol{J}_{\Omega a} & \boldsymbol{H}_{\Omega a}\\ \boldsymbol{J}_A - \boldsymbol{J}_{\Omega u} & \boldsymbol{H}_{\Omega u}\end{pmatrix}\begin{pmatrix}\dot{\boldsymbol{\Omega}}_a\\ \dot{\boldsymbol{u}}''\end{pmatrix}\end{aligned} \tag{42}$$

where each sub-matrix of the block matrix can be obtained from the following equations: $\boldsymbol{H}_{\mathrm{Tb}} = \sum_{k=1}^{N}\int_{A_k}{}^0\boldsymbol{T}_b{}^b\tilde{\boldsymbol{P}}_{ep}dm$; $\boldsymbol{J}_{Tb} = \sum_{k=1}^{N}\int_{A_k}\tilde{\boldsymbol{r}}_{ib}dm$; $\boldsymbol{J}_{\Omega b} = \sum_{k=1}^{N}\int_{A_k}\tilde{\boldsymbol{r}}_{ib}{}^0\boldsymbol{T}_b{}^b\tilde{\boldsymbol{P}}_{ep}dm$; $\boldsymbol{J}_{\Omega a} = \sum_{k=1}^{N}\int_{A_k}{}^0\boldsymbol{T}_e{}^e\tilde{\boldsymbol{r}}_p dm$; $\boldsymbol{H}_{\Omega a} = \sum_{k=1}^{N}\int_{A_k}{}^0\boldsymbol{T}_e\boldsymbol{S}_c dm$; $\boldsymbol{J}_{\Omega u} = \sum_{k=1}^{N}\int_{A_k}\tilde{\boldsymbol{r}}_{ib}{}^0\boldsymbol{T}_e{}^e\tilde{\boldsymbol{r}}_p dm$; and $\boldsymbol{H}_{\Omega u} = \sum_{k=1}^{N}\int_{A_k}\tilde{\boldsymbol{r}}_{ib}{}^0\boldsymbol{T}_e\boldsymbol{S}_c dm$.

In addition, except that the contact-impact forces yield between the two bodies of the system approaching to the deployed position, there are no external forces and torques to exert on the whole system. Therefore, according to conservation of linear and angular momentum, Eq. (42) can be represented in Jacobian matrix form of constraint equations as

$$\boldsymbol{\Phi}_2(\boldsymbol{q}) = \begin{pmatrix}\boldsymbol{P}\\ \boldsymbol{H}\end{pmatrix} = \boldsymbol{G}_q(\boldsymbol{q})\dot{\boldsymbol{q}} = \boldsymbol{0} \tag{43}$$

where the matrix $\boldsymbol{G}_q(\boldsymbol{q}) = \begin{pmatrix}m\mathbf{E}_3 & -\boldsymbol{H}_{Tb} & -\boldsymbol{J}_{\Omega a} & \boldsymbol{H}_{\Omega a}\\ -\tilde{\boldsymbol{r}}_b m_b + \boldsymbol{J}_{Tb} & \boldsymbol{J}_b + \boldsymbol{J}_A - \boldsymbol{J}_{\Omega b} & \boldsymbol{J}_A - \boldsymbol{J}_{\Omega u} & \boldsymbol{H}_{\Omega u}\end{pmatrix}$ is the Jacobian matrix. Thus, the dynamic equations including algebraic kinematic and momentum constraints considering the effect of contact-impact for the deployment and locking mechanism can be written as

$$\begin{aligned}&\boldsymbol{M}\ddot{\boldsymbol{q}} + \boldsymbol{K}\boldsymbol{q} + \boldsymbol{S}_q^T(\boldsymbol{q})\boldsymbol{\lambda}^s + \boldsymbol{G}_q^T(\boldsymbol{q})\boldsymbol{\lambda}^g = \boldsymbol{Q} - \boldsymbol{Q}_N + \boldsymbol{F}_n + \boldsymbol{F}_t \\ &\boldsymbol{\Phi}_1(\boldsymbol{q}) = \boldsymbol{0} \qquad \boldsymbol{\Phi}_2(\boldsymbol{q}) = \boldsymbol{0}\end{aligned} \tag{44}$$

Where $\boldsymbol{\lambda}^s$ and $\boldsymbol{\lambda}^g$ are the Lagrange multipliers for the constraints Eqs. (34) and (43), respectively, $\boldsymbol{F}_n$ and $\boldsymbol{F}_t$ are normal and tangential force vector, respectively, when the contact between the two bodies takes place, and the contact-impact model referred to by Lankarani and Nikravesh (1990) is given by

$$\boldsymbol{F}_n = (K_c\delta_{ij}^{1.5} + D_c\dot{\delta}_{ij})\cdot\boldsymbol{n}_{ij} \qquad \boldsymbol{F}_t = -\mu\|\boldsymbol{F}_n\|\cdot\boldsymbol{t}_{ij} \tag{45}$$

in which K_c and D_c = equivalent stiffness and equivalent damping constant, respectively; δ_{ij} = penetration depth; $\dot{\delta}_{ij}$ = relative impact velocity; μ = dynamic friction coefficient; and $\boldsymbol{n}_{ij}$ and $\boldsymbol{t}_{ij}$ = relative tangential and normal vectors of the contact point between the two bodies, respectively.

Numerical Simulations

In order to accurately predict the nonlinear mechanics behaviors of the deployment mechanism with laminated composite appendages

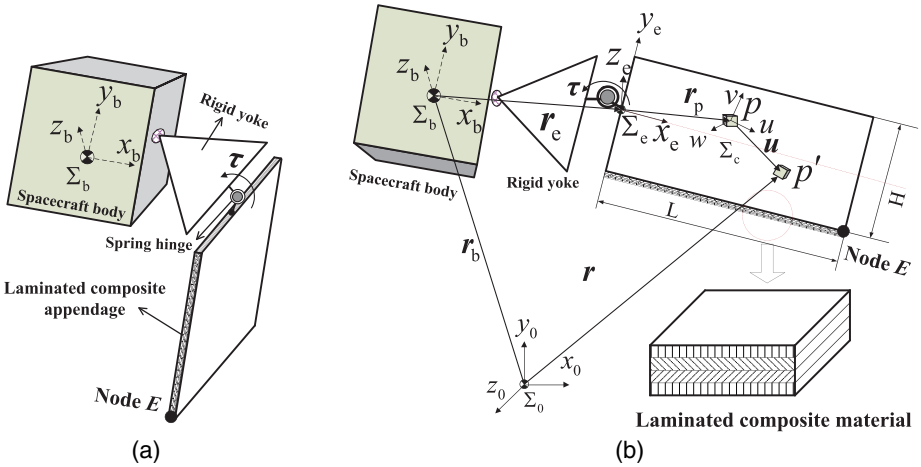

Fig. 5. Deployment and locking mechanism with flexible appendage

Table 1. Parameters of the Deployment Mechanism

Parameters	Size (m)	Mass (kg)	J_{xx} (kg · m^2)	J_{yy} (kg · m^2)	J_{zz} (kg · m^2)
Spacecraft body	$1.2 \times 1.2 \times 1.2$	3000	500	500	500
Rigid yoke	$0.3 \times 0.3 \times 0.3$	2.0	1.0	1.0	0.5
Flexible appendage	$2 \times 1.3 \times 0.002$	—	—	—	—

Table 2. Characteristics of the Two Lay-Ups Considered in the Applications of the Composite Appendage

Parameters	First layer	Second layer	Third layer	Fourth layer
Lay-up1	0°	0°	0°	0°
Lay-up2	0°	90°	90°	0°
Thickness (m)	0.0005	0.0005	0.0005	0.0005

according to the typical structure illustrated in Fig. 5, the dynamics properties of deployment and locking progress have been analyzed in this paper.

Large scale, low density, low stiffness, and flexibility appendages are often employed in aerospace engineering. Accordingly, the geometric and material properties of the appendage are described as follows: The grid yoke is equilateral triangle, and its length is 0.3 m. As shown in Fig. 2, the distances between the yoke and the spacecraft body and the appendage are: $\boldsymbol{l}_b = (0.8, 0, 0)$ m, and $\boldsymbol{a}_h = \boldsymbol{b}_h = (0.03, 0, 0)$ m, the initial location angle of hinge is 90°, and the final angle is 180° at deployed position. The basic geometric characteristics of the components of the appendage are presented by Anantharaman (1987). The centroid of each rigid body is assumed to be at the geometric center, and the main physical parameters are showed in Table 1. The appendage is 2.0 m long by 1.3 m wide and has a thickness of 2.0 mm, and it is made of a carbon fiber reinforced plastic with a specific mass of 1,600 kg/m^3, the composite material used in the model is a carbon reinforced plastic IM6/SC1081, the matrix is made of Epoxy SC1081 and the fiber of Carbon IM6. Note that the material used is not necessarily that of the real appendage, as the characteristics of such material are not publicly available. The properties of the composite material for a single layer with an orientation of 0 rad relatively to the X-axis are $E_1 = 177$ GPa; $E_2 = 10.8$ GPa; $G_{12} = G_{13} = 7.6$ GPa; $G_{23} = 8.504$ GPa; $\nu_{12} = 0.27$; and $\rho = 1{,}600$ kg/m^3. Two different laminates with four layers in each, described in Table 2, are considered.

The deployment mechanism is assumed to be at stowed position at the initial time. Initial conditions of this simulation study are listed as follows: All initial values for external forces and torques also are assumed to be zero. The parameters of the spring hinge as follows: The torsional stiffness $k_\theta = 80.0$ N · mm · (°)$^{-1}$, the initial deployment angle is assumed to be 90°, and preload torque $\tau_0 = 7{,}200.0$ N · mm. The equivalent contact stiffness is $K_c = 1 \times 10^6$ N · mm, the equivalent damping coefficient is $D_c = 1 \times 10^3$ N · s · mm^{-1}, and the dynamic friction coefficient is $\mu = 0.25$. To study the rigid-flexible coupled dynamic behavior of the system, the differential and algebraic equations (DAEs) of the motion are solved by using the Newmark method and Jacobian approach (Chen et al. 2012; Knupp et al. 2002). It has been proved that these methods not only can reduce the dimension of the equations of motion to improve the computational efficiency, but also obtain the better results with less constraint violation. At the same time, the calculation efficiency should be taken into account. Therefore, the reflection surface is modeled with 150 elements and 176 nodes in Fig. 6, which can achieve sufficient accuracy and higher efficiency. The simulations are studied by using the linear and nonlinear models. Furthermore, the simulation step size and time are 0.01 s and 30.0 s, respectively.

Fig. 7 shows the deployment angle of the flexible appendage for the linear and nonlinear models. It can be found that the deployment angle between the two bodies (yoke and appendage) reaches to 180° at time $t = 2.46$ s. Thus, it is indicated that the phenomenon of impact takes place for the first time as it was presented in the previous section. Accordingly, the rebound of the appendage reaches the peak value caused by impact forces. However, due to the effect of the damping and friction, the rebound amplitude of deployment angle decreases versus time. In Fig. 7 it is also observed that the value of the deployment angle is a little larger in the linear model than that of the nonlinear model since the nonlinear force $-\boldsymbol{Q}_N$ is ignored in the linear model. During deployment, a total of four impacts take place followed by rebounds, and at $t = 19.12$ s the steady-state of the appendage has been reached.

The same phenomena can be observed in the curve of torsional torque of the spring hinge represented by Fig. 8 for the linear and nonlinear models. According to $\tau = \tau_0 - k_\theta \theta$, at initial time torsional torque is $\tau = 7{,}200.0$ N · mm at stowed position. The elastic potential energy in the spring hinges is released and stored

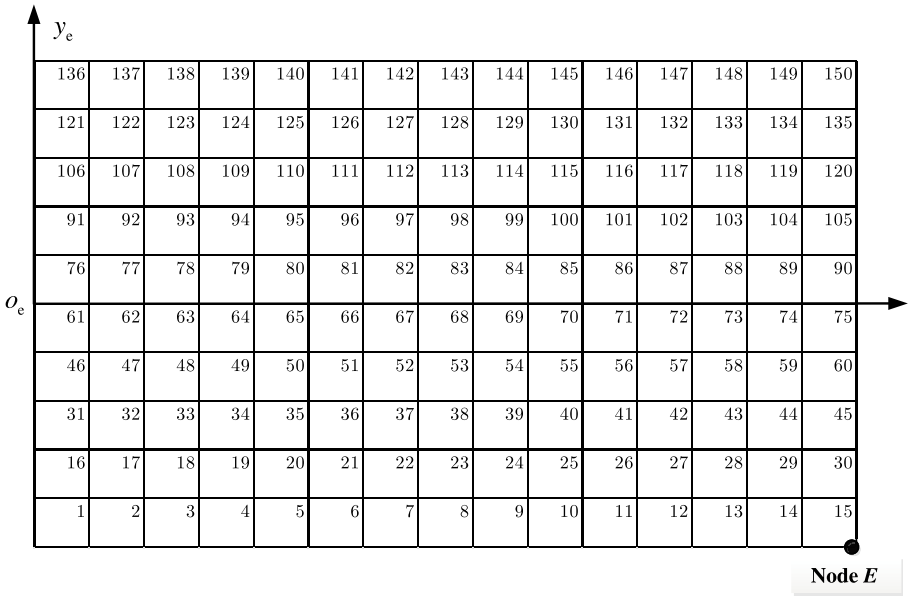

Fig. 6. Finite element division of laminated composite flexible appendage

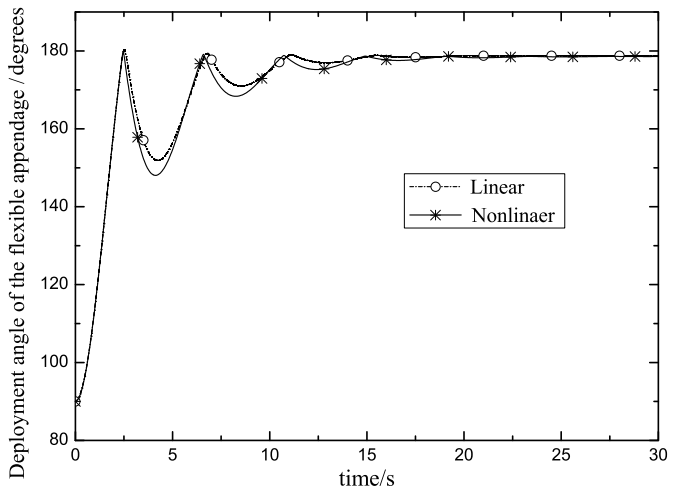

Fig. 7. Deployment angle of the flexible appendage

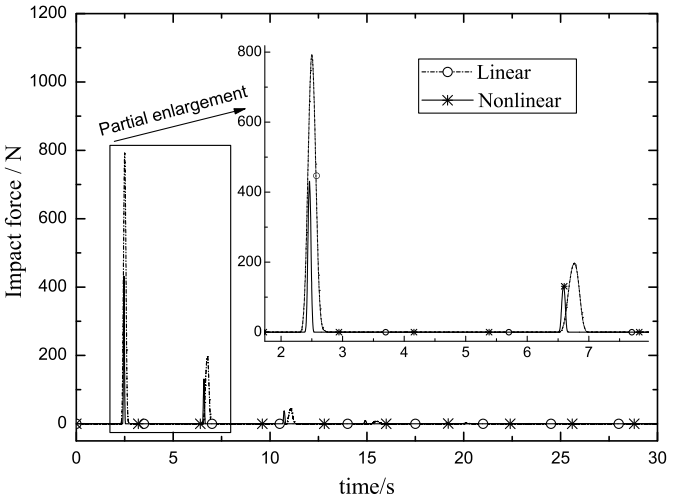

Fig. 9. Contact-impact forces of hinge

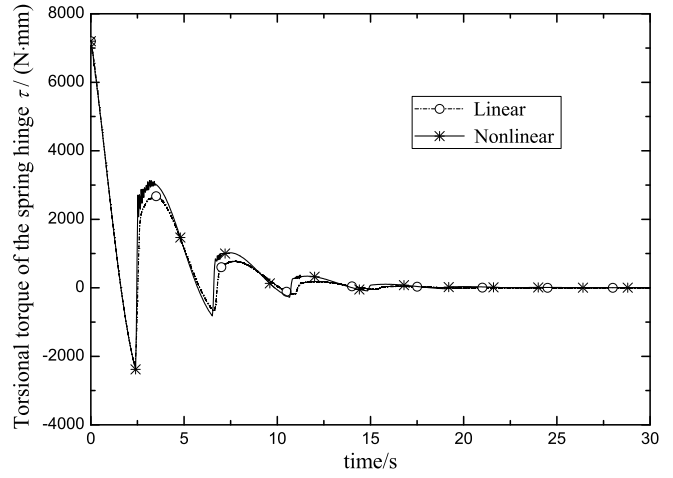

Fig. 8. Torsional torque of the spring hinge

repeatedly during deployment. Similarly, the value of the torsional torque is a little larger by the nonlinear model than that of the linear model versus deployment angle θ.

When the appendage is closed to the deployed position, the contact-impact is produced between the pin and curve locking groove as shown in Fig. 9. It can be observed that the effect of the hinge is obvious on the system's response. These peaks are associated with deployment angle closed to 180° as illustrated in Fig. 7. In addition, the nonlinear force $-\boldsymbol{Q}_N$ is ignored in the linear model leading to a relatively larger deployment velocity. Therefore, the peaks of the contact-impact are relatively low for the nonlinear model as observed in Fig. 9. Accordingly, the level of force peaks decrease with the effect of the damping and friction, which yields the less impacts. Finally, the dynamic system behavior tends to be steady-state after $t = 19.12$ s. This observation can be drawn by examination of Fig. 7 relative to the deployment angle.

Fig. 10 shows transverse deformation of the appendage on Node E. When the contact-impact forces occur between the pin and curve

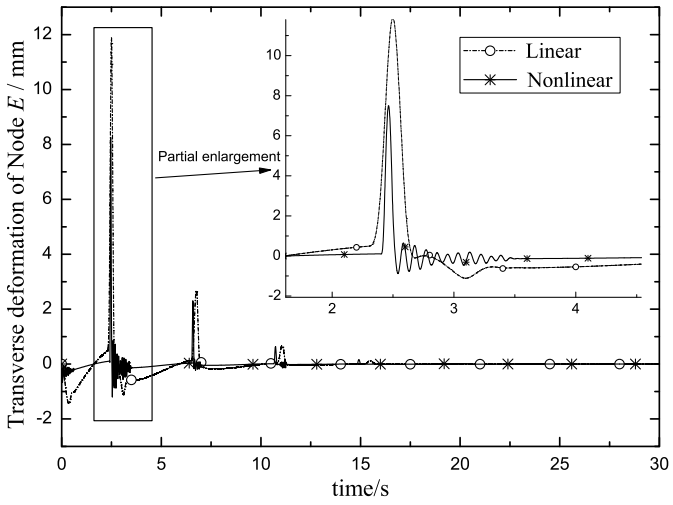

Fig. 10. Transverse deformation of Node E

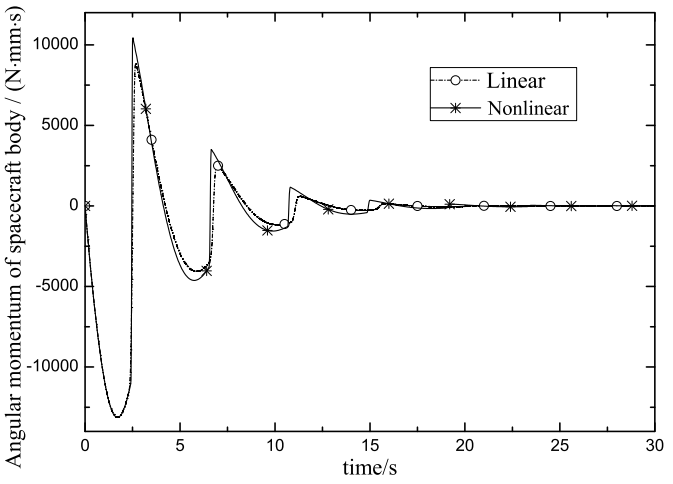

Fig. 12. Angular momentum of the spacecraft body

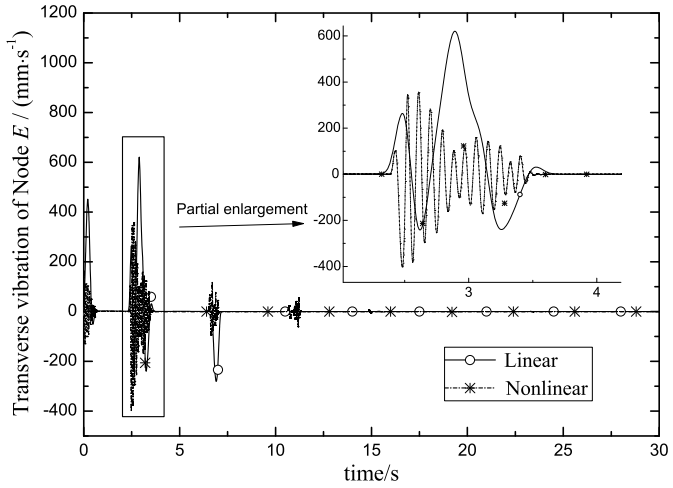

Fig. 11. Transverse vibration of Node E

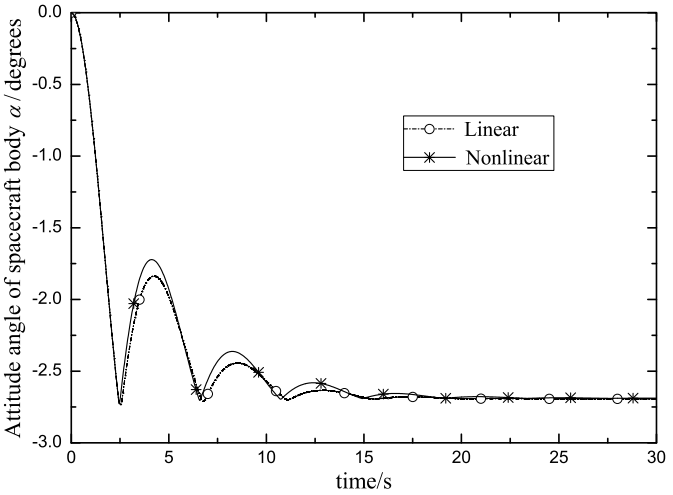

Fig. 13. Attitude angle of the spacecraft body

locking groove, the transverse deformation reaches peaks caused by contact-impact forces as perceived in Fig. 10. Furthermore, it can be observed that the contact-impact forces excite the nonlinear elastic deformation of flexible appendage, and it can lead to high-frequency flutter. Thus, it can be indicated that the deformation of the flexible appendage is sensitive to contact-impact forces.

Fig. 11 shows transverse vibration of Node E. It can be observed that the presence of nonlinear force $-\boldsymbol{Q}_N$ makes the peaks of vibration amplitude be lower in the nonlinear model than that of the linear model. However, as can be seen in Fig. 11, the vibration frequency is much larger in the present model. The differences between the two models are caused by the additional stiffness varying terms of $\boldsymbol{K}_s$ and $\boldsymbol{K}_L^*$. Such terms are ignored in the linear model leading to a stiffening shell structure of the appendage, which can yield improper divergent response with increasing of the angular velocity. Thus, the nonlinear forces $-\boldsymbol{Q}_N$, the nonlinear stiffening $\boldsymbol{K}_s$, and additional stiffness terms $\boldsymbol{K}_L^*$ will lead to the difference of the deformation and vibration of the flexible appendage between the linear model and the present model. All of these can change the results significantly for the system. Therefore, these results exhibit the reliability of the present modeling method for the mechanism composed of laminated composite appendage undergoing deployment and locking motions.

Due to the contact-impact forces, the spacecraft body is suffered angular momentum with interaction with other bodies shown as in Fig. 12. And since the mechanism is not exposed to external forces, its angular momentum is conserved according to Eqs. (36) and (37). Then, the peaks in angular momentum curve of the spacecraft body are consistent with numbers of impacts, which means that the numerical calculation is verified through simulation study. Because of the relatively larger mass of spacecraft body, it can be indicated that the contact-impact forces in very short moment have little influence on attitude angle as shown in Fig. 13. However, the neglect of $-\boldsymbol{Q}_N$, $\boldsymbol{K}_s$, and $\boldsymbol{K}_L^*$ can cause significant difference between the attitude angle obtained by two models, and the deviations will increase with deployment velocity. This difference is attributed to the effect of modeling error. Therefore, it is also revealed that the absence of nonlinear coupled terms can significantly influence the simulation results.

Conclusions

A dynamic modeling method is presented by using principle of virtual work in this paper which is suitable for predicting the dynamic behavior of a deployment and locking mechanism composed of

laminated composite appendage. The formulation employs a nonlinear elastic deformation field of plate/shell element to achieve the response of the laminated composite appendage. It can completely represent the geometrically nonlinear deformations, which contains the transverse and longitudinal deformations. These deformations are explicitly expressed in the formulations for capturing stiffness varying terms by the present modeling method, and it is developed by considering coupled deformation terms, the nonlinear stiffening, additional stiffness terms, and contact-impact forces. Thus, this methodology can provide the accurate dynamic model accounting for its nonlinear dynamic characteristics.

In addition, the contact-impact phenomenon is investigated located at the spring hinge, and a sudden force has a strong influence on the system during deployment. The linear and angular momentum model of the system is established in the absence of any external forces, which lead to conservation of linear and angular momentum. The geometric constraints yield as a result of restriction on the pin's motion on the surface of the locking groove. Accordingly, the Jacobian matrices of geometric and momentum constraints are derived from the hinge kinematics. Therefore, the generalized dynamical model is developed composed of a generalized constraint and contact-impact forces.

The comparison of the numerical simulation results between the linear model and the present model shows that the nonlinear model can exhibit the reliability for the dynamic behavior. In particular, it is revealed that coupled deformation terms, the nonlinear stiffening, additional stiffness terms, and contact-impact forces can significantly influence the simulation results during deployment, especially for the contact-impact arising from the spring hinge. However, the neglect of coupled and nonlinear terms in the linear model can cause significant improper response, and it can lead to producing erroneous results. And, it is illustrated that high-frequency oscillations of the appendage is sensitive to contact-impact forces since the complete expressions of coupled and nonlinear terms are included in the present modeling method. All simulation results indicate that the methodology for modeling and analysis of the system composed of laminated composite appendage are effective undergoing deployment and locking motions.

Acknowledgments

This material is based on Project 2013CB733000 supported by the National Basic Research Program of China, Project 51575126 supported by the National Natural Science Foundation of China, and Projects 2013M541358 and 2015T80358 supported by the China Postdoctoral Science Foundation.

References

Abe, A., Kobayashi, Y., and Yamada, G. (2000). "Non-linear vibration characteristics of clamped laminated shallow shells." *J. Sound Vib.*, 234(3), 405–426.

Abe, A., Kobayashi, Y., and Yamada, G. (2007). "Nonlinear dynamic behaviors of clamped laminated shallow shells with one-to-one internal resonance." *J. Sound Vib.*, 304(3-5), 957–968.

Anantharaman, M. (1987). "The dynamic analysis of flexible mechanisms using finite element methods." Ph.D. dissertation, Univ. of Stuttgart, Stuttgart, Germany.

Barut, A., Madenci, E., and Tessler, A. (1996). "Nonlinear elastic deformations of moderately thick laminated shells subjected to large and rapid rigid-body motion." *Finite Elem. Anal. Des.*, 22(1), 41–57.

Baz, A., and Ro, J. (2001). "Vibration control of rotating beams with active constrained layer damping." *Smart Mater. Struct.*, 10(1), 112–120.

Chandiramani, N. K., Librescu, L., and Shete, C. D. (2002). "On the free-vibration of rotating composite beams using a higher-order shear formulation." *Aerosp. Sci. Technol.*, 6(8), 545–561.

Chandiramani, N. K., Shete, C. D., and Librescu, L. (2003). "Vibration of higher-order-shearable pretwisted rotating composite blades." *Int. J. Mech. Sci.*, 45(12), 2017–2041.

Chen, S. L., Tan, K. K., and Huang, S. (2012). "Identification of coulomb friction-impeded systems with a triple-relay feedback apparatus." *IEEE T. Contr. Syst. T.*, 20(3), 726–737.

Du, H., Lim, M. K., and Liew, K. M. (1996). "Non-linear dynamics of multibodies with composite laminates. I: Theoretical formulation." *Comput. Method. Appl. M.*, 133(1-2), 15–24.

Fung, E. H. K., and Yau, D. T. W. (2004). "Vibration characteristics of a rotating flexible arm with ACLD treatment." *J. Sound Vib.*, 269(1-2), 165–182.

Fung, E. H. K., Zou, J. Q., and Lee, H. W. J. (2004a). "Lagrangian formulation of rotating beam with active constrained layer damping in time domain analysis." *J. Mech. Des.*, 126(2), 359–364.

Guo, X. Y., Zhang, W., and Yao, M. H. (2010). "Nonlinear dynamics of angle-ply composite laminated thin plate with third-order shear deformation." *Sci. China Technol. Sci.*, 53(3), 612–622.

Harras, B., Benamar, R., and White, R. G. (2002). "Geometrically nonlinear free vibration of fully clamped symmetrically laminated rectangular composite plates." *J. Sound Vib.*, 251(4), 579–619.

Knupp, P., Margolin, L., and Shashkov, M. (2002). "Reference Jacobian optimization-based rezone strategies for arbitrary Lagrangian Eulerian methods." *J. Comput. Phys.*, 176(1), 93–128.

Kremer, J. M., Shabana, A. A., and Widera, G. E. O. (1993a). "Large reference displacement analysis of composite plates. Part I: Finite element formulation." *Int. J. Numer. Meth. Eng.*, 36(1), 1–16.

Kremer, J. M., Shabana, A. A., and Widera, G. E. O. (1993b). "Large reference displacement analysis of composite plates. Part II: Computer implementation." *Int. J. Numer. Meth. Eng.*, 36(1), 17–42.

Lankarani, H. M., and Nikravesh, P. E. (1990). "A contact force model with hysteresis damping for impact analysis of multibody systems." *J. Mech. Des.*, 112(3), 369–376.

Lin, C. Y., and Chen, L. W. (2003). "Dynamic stability of a rotating beam with a constrained damping layer." *J. Sound Vib.*, 267(2), 209–225.

Liu, J. Y., and Hong, J. Z. (2002). "Dynamic modeling and modal truncation approach for a high-speed rotating elastic beam." *Arch. Appl. Mech.*, 72(8), 554–563.

Liu, J. Y., and Hong, J. Z. (2003). "Geometric stiffening of flexible link system with large overall motion." *Comput. Struct.*, 81(32), 2829–2841.

Liu, J. Y., and Hong, J. Z. (2004). "Dynamics of three-dimensional beams undergoing large overall motion." *Eur. J. Mech. A-Solid*, 23(6), 1051–1068.

Madenci, E., and Barut, A. (1996). "Dynamic response of thin composite shells experiencing nonlinear elastic deformations coupled with large and rapid overall motions." *Int. J. Numer. Meth. Eng.*, 39(16), 2695–2723.

Meirovitch, L. (1987). "Equations of motion for maneuvering flexible spacecraft." *J. Guid. Control Dyn.*, 10(5), 453–465.

Meirovitch, L., and Kwak, M. K. (1989). "State equations for a spacecraft with maneuvering flexible appendages in terms of quasi-coordinates." *Appl. Mech. Rev.*, 42(11), S161–170.

Messina, A., and Soldatos, K. P. (2002). "A general vibration model of angle-ply laminated plates that accounts for the continuity of interlaminar stresses." *Int. J. Solids Struct.*, 39(3), 617–635.

Modi, V. J. (1974). "Attitude dynamics of satellite with flexible appendages—A brief review." *J. Spacecr. Rockets*, 11(11), 743–751.

Neto, M. A., Ambrosio, J. A. C., and Leal, R. P. (2004). "Flexible multibody systems models using composite materials components." *Multibody Syst. Dyn.*, 12(4), 385–405.

Neto, M. A., Ambrosio, J. A. C., and Leal, R. P. (2006). "Composite materials in flexible multibody systems." *Comput. Meth. Appl. M.*, 195(50-51), 6860–6873.

Topal, U., and Uzman, Ü. (2010). "Effect of rectangular/circular cutouts on thermal buckling load optimization of angle-ply laminated thin plates." *Sci. Eng. Compos. Mater.*, 17(2), 93–110.

You, B. D., Zhao, Z. G., and Zhao, Y. (2010). "Disturbance analysis and suppression of flexible antenna reflector on free-floating satellite antenna." *Acta Aeronaut. Astronaut. Sinica*, 31(12), 2348–2356.

Zhang, W. (2001). "Global and chaotic dynamics for a parametrically excited thin plate." *J. Sound Vib.*, 239(5), 1013–1036.